GEOCHEMISTRY

Diamond formation in an electric field under deep Earth conditions

Yuri N. Palyanov[1,2]*, Yuri M. Borzdov[1], Alexander G. Sokol[1], Yuliya V. Bataleva[1], Igor N. Kupriyanov[1], Vadim N. Reutsky[1], Michael Wiedenbeck[3], Nikolay V. Sobolev[1,2]

Most natural diamonds are formed in Earth's lithospheric mantle; however, the exact mechanisms behind their genesis remain debated. Given the occurrence of electrochemical processes in Earth's mantle and the high electrical conductivity of mantle melts and fluids, we have developed a model whereby localized electric fields play a central role in diamond formation. Here, we experimentally demonstrate a diamond crystallization mechanism that operates under lithospheric mantle pressure-temperature conditions (6.3 and 7.5 gigapascals; 1300° to 1600°C) through the action of an electric potential applied across carbonate or carbonate-silicate melts. In this process, the carbonate-rich melt acts as both the carbon source and the crystallization medium for diamond, which forms in assemblage with mantle minerals near the cathode. Our results clearly demonstrate that electric fields should be considered a key additional factor influencing diamond crystallization, mantle mineral–forming processes, carbon isotope fractionation, and the global carbon cycle.

INTRODUCTION

Established models for diamond genesis are based primarily on mineralogical and geochemical studies of natural diamonds, thermodynamic modeling, and results of experiments on diamond crystallization in model systems (*1*–*6*). Currently, most scientists recognize that diamond formation is polygenic in nature (*4*–*6*), involving various (i) carbon sources and crystallization media (*7*–*16*) such as C—O—H (±N±S) fluids, carbonate melts/fluids, carbonates, and carbides or metal-carbon melts; (ii) *P-T-fO*$_2$*-pH* conditions of formation (*4*–*6*, *12*, *17*, *18*); and (iii) processes, mechanisms/driving forces of crystallization (*4*–*6*, *12*, *19*–*21*). According to broadly accepted models (*2*, *4*), diamond formation occurs in a course of mantle metasomatic processes and concomitant redox reactions resulting in the oxidation of hydrocarbons or the reduction of CO_2 to elemental carbon. Other diamond formation models emphasize decompression or cooling of fluids (*22*), a partial melting in the presence of a fluid (*23*, *24*), a *pH* drop during fluid-rock interactions without changes in oxidation state (*17*), or mixing of different fluids or melts (*3*, *17*).

Despite the many theoretical, thermodynamical, and experimental works devoted to the investigation of diamond, key aspects related to the driving forces or "triggers" of diamond formation remain debated. Several diamond formation mechanisms have been experimentally studied, including redox reactions involving carbonates and Si, SiC or silicon-bearing metal alloys (*25*, *26*), decarbonation reactions with a subsequent reduction of CO_2 by reduced fluids (*27*, *28*), or sulfides (*29*, *30*), as well as carbonate-iron interaction (*19*–*21*). Given the huge diversity of natural diamonds in terms of morphology, inclusion mineralogy, age, petrological settings, and relationships with global geodynamic processes, one may suppose that diverse mechanisms (driving forces) may be responsible for diamond formation. In this connection, experimental investigations of different factors capable of affecting diamond formation deserve special attention. Of particular interest is the behavior of carbon and carbon-bearing compounds in the presence of redox gradients or electrochemical potentials.

Our work is based on the hypothesis that an electrochemical process may be involved in diamond formation in Earth's mantle, which is supported by the high electrical conductivity of mantle melts and fluids (*31*–*33*), in conjunction with electrochemical processes supposedly active in Earth's interior (*34*–*36*). We hypothesize that these chemically induced voltage gradients can be associated with both magnetic field variations (*37*, *38*) and lateral or vertical redox heterogeneity in the mantle (*39*, *40*). To assess the possibility of inducing diamond formation in mantle media via the action of an electric field, we designed special high-pressure electrochemical cells and conducted experiments in model media having compositions based on the reported inclusions in natural diamonds (*7*–*10*). In this work, we focus only on carbonate, carbonate-silicate, and water-carbonate-silicate media under pressure-temperature (*P-T*) conditions of the lithospheric mantle and assess the role of the electrochemical potential as one of the possible factors for diamond formation in Earth's upper mantle.

RESULTS AND DISCUSSION

Experiments on the crystallization of diamond and graphite in the presence of an electric potential field were performed at pressures of 6.3 and 7.5 GPa, in the temperature range of 1300° to 1600°C, and with potential difference between the electrodes ranging from 0.4 to 1 V (see Materials and Methods for details). The electrochemical high-pressure cells designed for this study are presented in Fig. 1. In all experiments, the heating of the reaction chamber to the required temperature was accomplished using a graphite heater, which was electrically and chemically isolated from the samples. The electrochemical gradient was provided via an independent electrical circuit shown in Fig. 1. The experimental conditions and results, including the observed changes in phase compositions of the samples from the cathode to the anode, are presented in Table 1. The chemical compositions of the produced phases are reported in table S1.

[1]V.S. Sobolev Institute of Geology and Mineralogy, Siberian Branch of the Russian Academy of Sciences, Academician Koptyug Ave., 3, Novosibirsk 630090, Russian Federation. [2]Novosibirsk State University, Pirogova str., 2, Novosibirsk 630090, Russian Federation. [3]Deutsches GeoForschungsZentrum, 14473 Potsdam, Germany. *Corresponding author. Email: palyanov@igm.nsc.ru

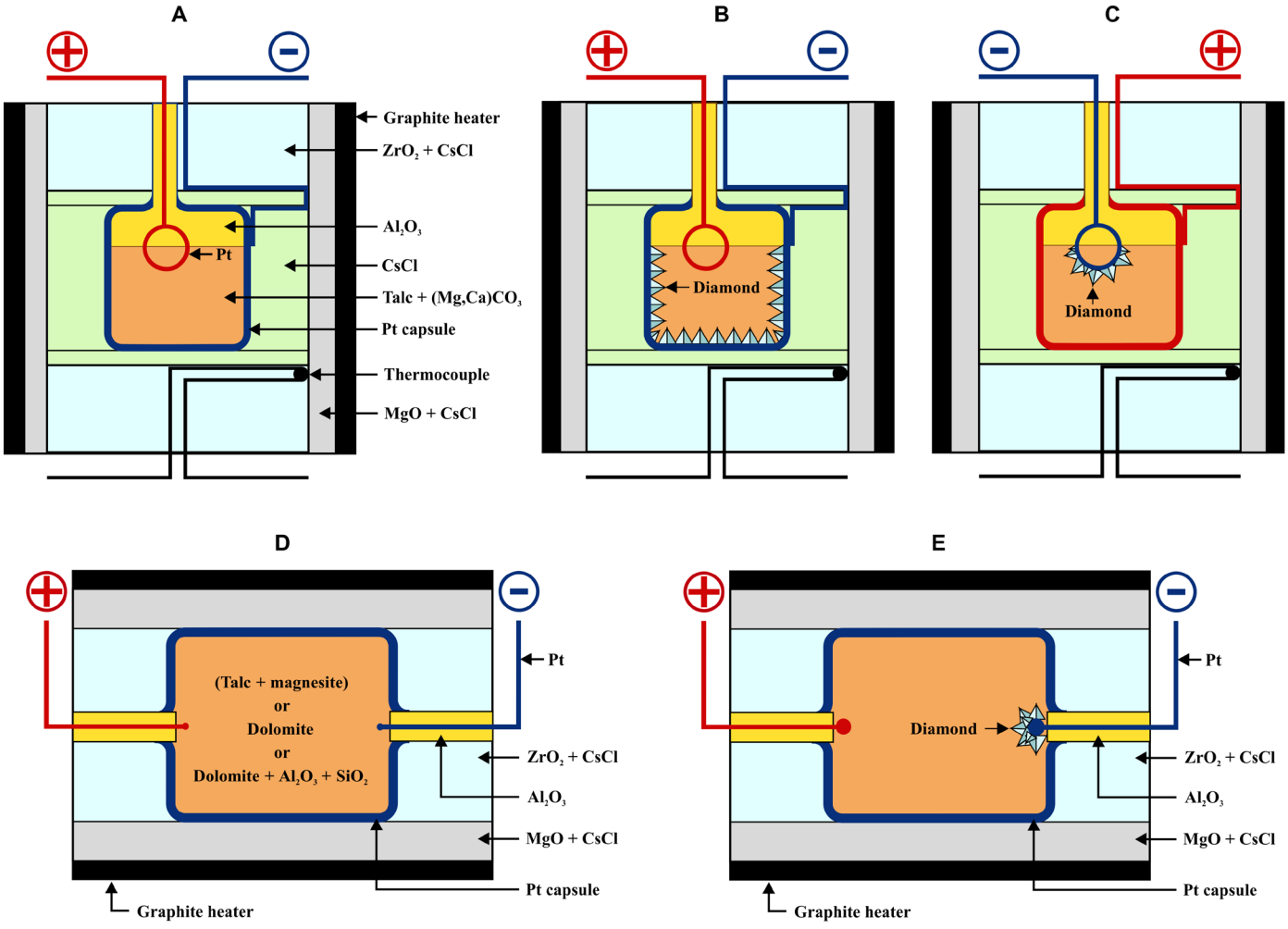

Fig. 1. Electrochemical cell assemblies used in experiments with model media under mantle *P-T* conditions. (**A**) Vertical assembly, (**B**) vertical assembly after experiments with the localization of diamond at the Pt capsule (cathode), (**C**) vertical assembly after experiments with the localization of diamond at the Pt loop (cathode), (**D**) horizontal assembly, and (**E**) horizontal assembly after experiments with the localization of diamond at the Pt loop (cathode).

Table 1. Experimental conditions and results.

Run (#)	Initial composition*	*P* (GPa)	*T* (°C)	Time (hours)	*U* (V)	Phase assemblages of zones† (from cathode to anode)
1229	Ms (60 mg), Ta (60 mg)	6.3	1300	15	0.95	[Gr] → [L_1 + Gr] → [En + L_1] → [En + Ms]
2085	Ms (122 mg), Ta (122 mg)	7.5	1500	15	0.4	[En + L_1 + Dm + Gr] → [En + Ms + L_1]
2097	Ms (120 mg), Ta (120 mg)	7.5	1500	15	0	[En + Di + Co + Ms + L_1]
1258	Ms (60 mg), Ta (60 mg)	7.5	1550	15	1	[L_1 + Dm + Gr] → [En + Ms + L_1]
1251	Ms (60 mg), Ta (60 mg)	7.5	1600	15	1	[L_1 + Dm + Gr] → [En + Ms + L_1]
643	Dol (1327 mg)	6.3	1500	6	1	[Pc + Gr + Mg,Ca-carb] → [L_2]
1205	Dol (670 mg)	7.5	1500	15 + 2‡	1	[Pc + Gr + Dm + Mg,Ca-carb] → [L_2]
1212	Dol (670 mg)	7.5	1600	16	1	[Pc + L_2 + Gr + Dm] → [L_2]
1267	Dol (60 mg), Di (60 mg)	7.5	1600	15	1	[L_3 + Dm + Gr + Di + Fo] → [Di + L_3] → [Di]
642	Dol (760 mg), SiO_2 (300 mg), Al_2O_3 (267 mg)	6.3	1500	40	1	[Grt + Dm + Gr + Cor + L_3] → [L_3]

*Ms: magnesite, $Mg_{0,9}Ca_{0,1}CO_3$; Ta: talc, $Mg_3Si_4O_{10}(OH)_2$; Dol: dolomite, $CaMg(CO_3)_2$. †En, enstatite; L_1, quenched water-bearing carbonate-silicate melt; Dm, diamond; Gr, metastable graphite; Co, coesite; L_2, quenched carbonate melt; Pc, periclase; Di, diopside; Grt, garnet; L_3, quenched carbonate-silicate melt; Fo, forsterite; Cor, corundum. ‡Experiment was performed by holding the sample at 1500°C for 15 hours, followed by a gradual temperature decrease to 1000°C over 2 hours. U: V, potential difference at the electrodes (volts).

In experiments with a water-bearing carbonate-silicate melt (talc + Ca-magnesite system), diamond and/or metastable graphite were produced in assemblage with pyroxene, recrystallized magnesite, and a carbonate-silicate melt. The recovered samples show a systematic zoning in the phase composition from one electrode to another. At 1300°C and 6.3 GPa, the phase composition of the zones changes in following sequence from the cathode to the anode: (i) metastable graphite → (ii) carbonate-silicate melt (Ca # 0.29) with metastable graphite → (iii) enstatite and diopside with interstitial quenched melt → (iv) recrystallized magnesite and enstatite. Note that the degree of partial melting in all experiments did not exceed 20 weight % (wt %). At 1500°C and 7.5 GPa, an assemblage of diamond, metastable graphite, and enstatite coexisting with carbonate-silicate melt (Ca # 0.38) was produced at the cathode (Fig. 2, A and B, and fig. S1, A to E), whereas, at the anode, diamond and graphite did not form. In a control experiment performed with the same starting composition but in the absence of any applied electric field, neither graphite nor diamond was produced. The recovered sample consisted of enstatite, diopside, coesite, and magnesite coexisting with a carbonate-silicate melt (Ca # 0.44) (fig. S1F). At 1550° and 1600°C, diamond (fig. S2A), metastable graphite, and a melt were formed at the cathode, whereas enstatite (fig. S2B), magnesite, and a melt were present in the area adjacent to the anode (fig. S1, G to I). The crystallized diamonds have an octahedral morphology and reach up to 200 μm in size in runs at 1550° and 1600°C. From the infrared (IR) absorption analysis, it is found that those diamond crystals contain nitrogen impurities in the form of N-related point defects comprising isolated substitutional nitrogen atoms (C centers) and nearest-neighbor substitutional nitrogen pairs (A centers) (Fig. 3). The calculated nitrogen concentrations are within the range of 1000 to 1200 atomic parts per million (ppm), and the degree of nitrogen aggregation from the single C-form to the paired A-form is 25 to 30%. The IR spectra also show absorption bands associated with inclusions of silicates (1080 to 900 cm^{-1}) and carbonates (1440 to 1450 cm^{-1}).

In experiments with dolomite conducted at 1500°C, it was found that diamond and/or metastable graphite crystallized at the cathode in assemblage with periclase and Mg,Ca carbonate (Ca # 0.04 to 0.1). To better understand the phase formation processes induced through the application of the voltages, we performed one of our experiments (#1205) by holding the sample at 1500°C for 15 hours, followed by a gradual temperature decrease to 1000°C over 2 hours. During this experiment, periclase, graphite, and carbonate formed a polycrystalline aggregate surrounding the cathode (Figs. 2, C and D, and 4 and fig. S3, A to C). In contrast, other parts of the capsule distal to the cathode consisted solely of a crystallized high-Ca carbonate melt (Ca # 0.79). At 1600°C, diamond, graphite, and periclase crystallized with a coexisting carbonate melt matrix (Ca # 0.39) in proximity to the cathode (fig. S3, D and E), while a melt formed in other parts of the sample had Ca # 0.61. Figure 4A reports the contrasting distribution of the phases produced across the Pt capsule. Chemical distribution maps (Fig. 4, B to D) also show systematic patterns that are spatially associated with the applied electric potential difference. Diamond crystallized both directly at the cathode and in the melt in the areas adjacent to the cathode. Crystallized octahedral diamonds up to 100 to 120 μm in size contain nitrogen impurities in the form of C and A centers with a total concentration of 450 to 550 atomic ppm (Fig. 3) and an aggregation degree of 10 to 15%. A prominent absorption band associated with carbonate inclusions (1430 to 1440 cm^{-1}) is present in the IR spectra (Fig. 3).

Experiments simulating the behavior of anhydrous carbonate-silicate melts in the presence of an electric field were performed both with dolomite + diopside and with dolomite + SiO_2 + Al_2O_3

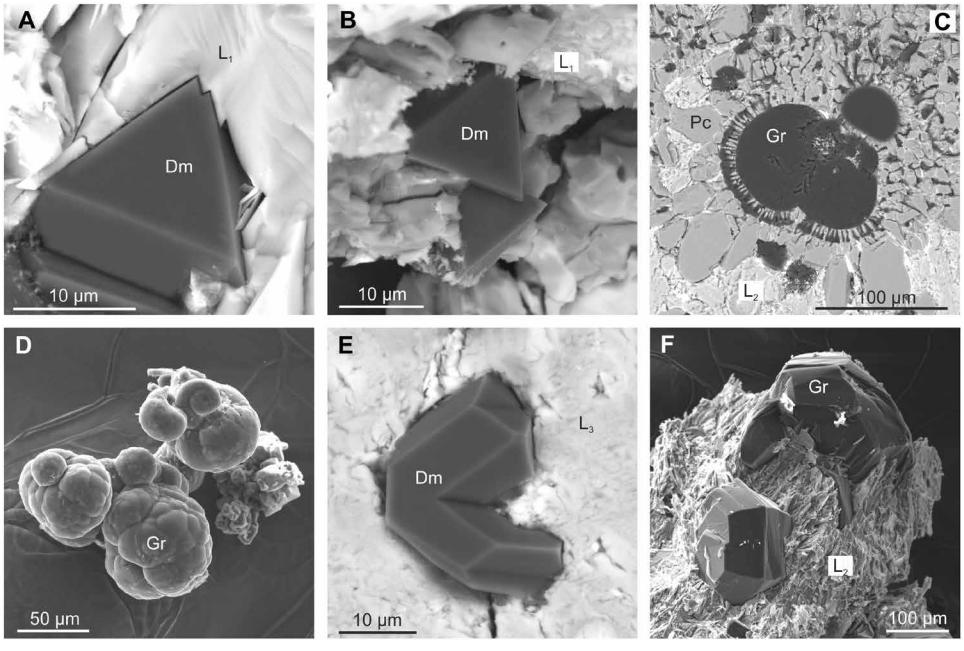

Fig. 2. Scanning electron microscopy images of diamond and graphite crystallized in electrochemical experiments. Scanning electron microscopy (SEM) micrographs were taken in backscattered electron mode for samples produced in experiments with (**A** and **B**) quenched water-bearing carbonate-silicate melts (run #2085, 7.5 GPa, 1500°C), (**C** and **D**) quenched carbonate melts (run #1205, 7.5 GPa, 1500°C), (**E**) quenched carbonate-silicate melts (run #1267, 7.5 GPa, 1600°C), and (**F**) quenched carbonate-silicate melts (run #642, 6.3 GPa, 1500°C). L_1, quenched water-bearing carbonate-silicate melt; L_2, quenched carbonate melt; L_3, quenched carbonate-silicate melt; Pc, periclase; Gr, graphite; Dm, diamond.

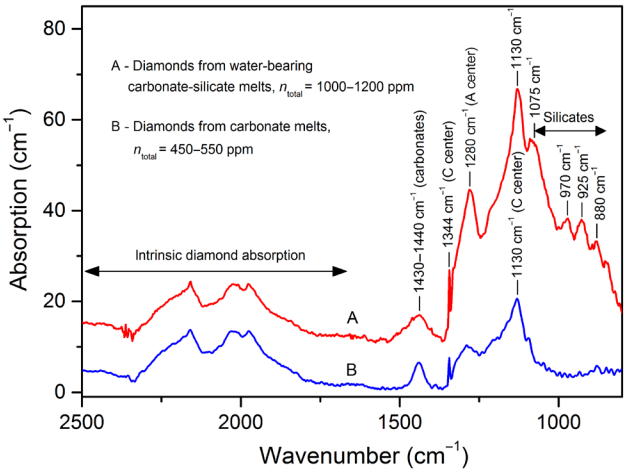

Fig. 3. Typical IR absorption spectra of crystallized diamonds. The spectra were acquired from diamond crystals produced in experiments with (**A**) water-bearing carbonate-silicate melts and (**B**) carbonate melts. The spectra have been vertically offset for clarity.

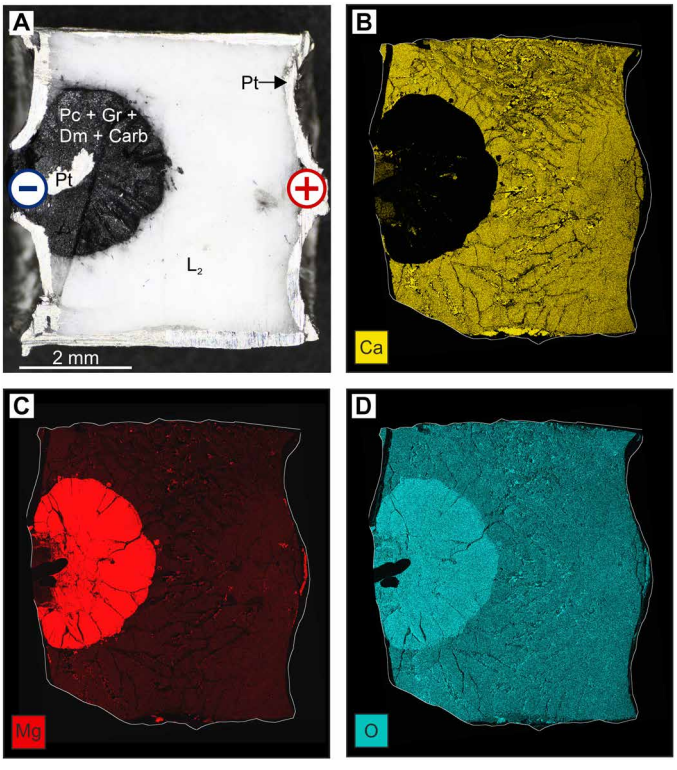

Fig. 4. Optical and energy-dispersive spectrometry investigations. (**A**) Photomicrograph of a sample (cross section) after an experiment with the dolomite starting composition (run #1205, 7.5 GPa, 1500°C). (**B** and **C**) Chemical maps showing distribution of (B) Ca, (C) Mg, and (**D**) O over the sample. Carb, Mg,Ca carbonate.

starting compositions. In the dolomite-diopside system at 7.5 GPa and 1600°C, diamond, graphite, forsterite, and recrystallized diopside formed in coexistence with a carbonate-silicate melt (fig. S4, A to E). Diamond and graphite crystallized both at the cathode (Pt capsule) (Fig. 2E and fig. S4, F to I) and in the adjacent areas in an assemblage with diopside, forsterite, and a carbonate-silicate melt (Ca # 0.55). The central part of the sample contained diopside crystals coexisting with the quenched melt (Ca # 0.65). Macrocrystalline diopside was found adjacent to the anode. The sample recovered from the experiment at 6.3 GPa and 1500°C for 40 hours with the dolomite + SiO_2 + Al_2O_3 starting composition also records a pronounced compositional zoning. Diamond and graphite (Fig. 2F) crystallized in assemblage with the pyrope-grossular garnet (Ca # 0.27) and carbonate-silicate melt (Ca # 0.65) were found only near the cathode (fig. S5, A to E). Only a carbonate-silicate melt was found in the areas adjacent to the anode. Produced diamonds have an octahedral morphology and reach up to 120 to 150 μm in size. IR absorption measurements reveal that the diamond crystals contain nitrogen impurity in the form of C and A centers with a total concentration of 600 to 700 atomic ppm and an aggregation degree of 15 to 20%. The IR spectra also exhibit absorption bands due to carbonate and silicate inclusions.

Carbon isotope analyses (table S2) reveal that the crystallized diamond and graphite are depleted in ^{13}C relative to the parental carbonate and carbonate-silicate melts. The observed magnitude of the C isotope fractionation is on average 5.4 and 5.9 per mil (‰) for the carbonate and water-containing carbonate-silicate systems, respectively. In the case of the anhydrous carbonate-silicate melt, the value of the isotopic fractionation reaches 9.2‰. Our results unambiguously indicate that the crystallization of diamond and graphite through the reduction of carbon from carbonate in an applied electric field is accompanied by a substantial carbon isotope fractionation. The measured fractionation significantly exceeds the expected value predicted by thermodynamic equilibrium, which, for a carbonate-graphite pair, should be 1.2 to 1.6‰ at 1300° to 1600°C (*41*).

Thus, the experiments described here reveal that an electric field, when applied to the mantle fluids and melts, can induce the reduction of carbon from carbonates, mass transfer of carbon in carbonate and carbonate-silicate melts, and crystallization of diamond and/or graphite. The mechanism(s) by which an electric field induces carbon generation and diamond crystallization can be reconstructed on the basis of the obtained experimental results and published data. As mantle carbonate and carbonate-silicate melts contain anionic CO_3^{2-} groups (*42*, *43*), the process of carbon reduction under high-pressure high-temperature (HPHT) conditions is likely similar to electrolytic deposition of carbon from carbonate melts implemented at ambient pressure (*44*, *45*). For the dolomite composition, the reactions are as follows. At the cathode

$$CO_3^{2-} + 4\bar{e} \rightarrow C^0 + 3O^{2-} \quad (1)$$

$$Mg^{2+} + O^{2-} \rightarrow MgO \quad (2)$$

The oxide ion (O^{2-}) formed by the reaction 1 is transported to the anode, where it reacts by

$$2O^{2-} \rightarrow 4\bar{e} + O_2\uparrow \quad (3)$$

Oxygen formed by the reaction 3 can partly be dissolved in the carbonate melt, leading to high oxygen fugacity near the anode. It is also possible that a part of molecular oxygen can escape from the capsule due to the leakages at the interface between the Pt capsule and the electrode(s).

For the water-bearing carbonate-silicate composition (magnesite + talc), we suppose that in addition to reactions 1 and 2, water

dissolved in the melt undergoes partial dissociation with subsequent H_2 formation at the cathode. Carbon and oxygen formed by the reactions 1 and 3, respectively, may react with each other to produce carbon dioxide

$$C + O_2 \rightarrow CO_2 \quad (4)$$

According to experimental data, the solubility of CO_2 in carbonate and carbonate-silicate melts can reach a level of tens of percent (*46*–*48*). Then, near the cathode in melts with dissolved CO_2, the following reaction may take place

$$CO_2 + 2H_2 \rightarrow C + 2H_2O \quad (5)$$

The feasibility of the reaction 5, leading to diamond formation, has been documented by experiments on decarbonation using external sources of hydrogen (*28*, *49*). Owing to the reactions 1 and 5, carbon saturation is established in the melt, and, accordingly, crystallization of diamond or graphite near the cathode becomes a favorable pathway as electric current continues to flow through the system. The reduction of carbon (C^0) from a carbonate-bearing melt by reaction 1 inevitably leads to excess O^{2-} and a shift in the ratios of anionic CO_3^{2-} groups to divalent cations (Ca^{2+} and Mg^{2+}) in the melt. Therefore, diamond and/or graphite crystallize in assemblage with oxide or silicate phases.

The recognition that electric potentials significantly affect mineral stability fields implies that this new diamond forming pathway may be an important factor within the global carbon cycle (*50*, *51*). Carbon isotope ratio determinations show that the electrochemical reduction of carbon from carbonates and the subsequent crystallization of diamond or graphite leads to significant isotopic fractionation of carbon, far exceeding the scale of equilibrium fractionation of carbon isotopes between diamond or graphite and carbonate under mantle *P*-*T* conditions. We suggest that electrochemical crystallization can be an important mechanism leading to the formation of isotopically light carbon and resulting in graphite and diamond with C isotopic compositions down to −15‰ as compared to carbonate with a typical mantle C isotopic composition ($\delta^{13}C_{PDB} = -5 \pm 2‰$) (*4*). Using the analogy of electrochemical fractionation of Fe isotopes (*52*) suggests that kinetic effects may have a role in the observed carbon isotope fractionation. In both cases, light isotopes migrate faster, resulting in an isotopically lighter end product. If confirmed, then one could expect voltage dependence for the carbon isotope fractionation, but, with the current dataset, we cannot confirm this. On the other hand, diamond or graphite is always lighter than carbonate due to thermodynamic effects during isotope fractionation [e.g., (*41*, *53*)].

Our experiments have documented that electric fields can affect mineral-forming processes under mantle *P*-*T* conditions. However, available research provides little information concerning possible values for the electrical fields in Earth's mantle. A detailed analysis of the driving force for chemical reactions and charge transfer reactions in the deep zones of Earth was given by Kavner and Walker (*36*). In a subsequent paper, Kavner *et al.* (*54*) showed that at 20 kbar and 1400°C, a 1-V potential drop across synthetic basalt induces effective oxygen fugacity perturbations of 10 orders of magnitude. Under mantle conditions, this electrochemical disequilibrium can be expected when two different phase assemblages that are not in redox equilibrium with each other are brought into contact. The oxygen fugacity gradient modeling the potential difference of 0.4 to 1 V [oxygen potential difference between Fayalite-Magnetite-Quartz and Iron-Wustite buffers (ΔFMQ-IW) circa 5 log units and oxygen potential difference between Magnetite-Hematite and Iron-Wustite buffers (ΔMH-IW) circa 9 log units] may arise when highly oxidized subduction fluids penetrate into the metal-bearing mantle. Theoretical chemical mass transfer calculations show that the breakdown of antigorite to olivine, enstatite, and chlorite in a subducting slab can generate fluids with high oxygen fugacities, close to the hematite-magnetite buffer (*55*). Were these oxidized fluids (fO_2 ~ MH) to come into contact with metal-containing peridotite (fO_2 ~ IW), the fugacity gradient could reach 9 log units. Under these conditions, electrochemical disequilibrium at a fluid/solid interface may reach 1 V.

We have demonstrated that exposing mantle analogous diamond-forming media to an electric field results both in the reduction of carbon from carbonates and the subsequent crystallization of diamond alongside of mantle minerals. In the studied carbonate and carbonate-silicate systems, carbonates act both as the carbon source and as the main component of diamond crystallization medium. We note that some characteristics of the synthesized diamonds—an octahedral morphology, relatively high nitrogen content of ~1000 atomic ppm and the presence of silicate-carbonate inclusions—are features commonly observed for type Ia natural diamonds. Note that apart from the essential relevance to modeling natural diamond–forming processes, the experimental approach reported in this study can be useful for elucidating the thermodynamic behavior of carbon redox processes at high pressure and temperature and for gaining information about chemical partitioning/distribution between phases subjected to a redox gradient.

MATERIALS AND METHODS

Experimental design

Experiments were carried out at V.S. Sobolev Institute of Geology and Mineralogy, Siberian Branch of the Russian Academy of Sciences (SB RAS) (Novosibirsk, Russia) using a split-sphere multianvil high-pressure apparatus (BARS) (*56*) at pressures ranging from 6.3 to 7.5 GPa, temperatures in the range of 1300° to 1600°C, and run duration between 6 and 40 hours. To investigate the effect of the applied electric potential difference, we developed high-pressure electrochemical cells. These cells were based on high-pressure cells in the form of tetragonal prisms, calibrated at pressures of 6.3 and 7.5 GPa (*57*, *58*).

The electric potential difference applied between the electrodes ranged from 0.4 to 1 V. Both vertical and horizontal assemblies for high-pressure electrochemical cells were developed (Fig. 1).

In the vertical assembly (Fig. 1, A to C), the electrodes were a platinum capsule and a platinum loop electrically isolated from the capsule using Al_2O_3. In the horizontal assembly (Fig. 1, D and E), isolated platinum electrodes (0.2 to 0.3 mm in diameter) were inserted into a Pt capsule with the starting sample materials. For the cell calibrated at 6.3 GPa, the diameter of the Pt capsule was 8 mm, and at 7.5 GPa, it was 6 mm. In all the developed designs of the electrochemical cells, six possible independent electrical contacts are involved: two for the graphite heater, two for applying an electric potential difference, and two for enabling temperature measurements using a PtRh 30/6 thermocouple. Initial testing of the cell designs involved several trial experiments performed using a vertical assembly scheme. Using identical assembly designs, starting compositions, and *P*-*T* conditions, the effect of changing the polarity of the applied potential

difference was examined (Fig. 1, B and C). These tests conclusively showed that our capsule designs yielded reproducible results. In particular, diamond was found to crystallize exclusively at the cathode irrespective of whether the Pt capsule or Pt loop was negatively biased.

The developed high-pressure cells enable prolonged (up to 40 hours) electrochemical experiments over a wide range of *P-T* conditions using capsules with relatively large volumes. The design features of the BARS devices made it possible to use both vertical and horizontal crystallization schemes in conjunction with multichannel measurements. It ensures a stable heating of the samples, reliable temperature measurements, and the provision of constant potential differences to the model media in the electrochemical cells. To the best of our knowledge, such an experimental technique has not been previously reported.

Starting materials

To model diamond-forming media, water-bearing and water-free carbonate-silicate and carbonate melts, we used the following starting compositions (Table 1): (i) a mixture of talc $Mg_3Si_4O_{10}(OH)_2$ and Ca-bearing magnesite $(Mg_{0,9}Ca_{0,1})CO_3$ in a 1:1 weight ratio; (ii) dolomite $CaMg(CO_3)_2$; (iii) a mixture of dolomite $CaMg(CO_3)_2$ and diopside $CaMgSi_2O_6$ in a 1:1 weight ratio; and (iv) a mixture of dolomite $CaMg(CO_3)_2$, Al_2O_3, and SiO_2. Starting materials consisted of natural specimens of magnesite and dolomite (Satka deposit, Chelyabinsk region, Russia) and talc (Irkutsk region, Russia) with total impurities of <0.5 wt % along with powders of chemically pure synthetic diopside, Al_2O_3, and SiO_2. In all experiments, the capsules were loaded with a homogeneous mixture of the starting reagents. Diamond seed crystals were not used in any experiment. The reason for this is that to analyze the isotopic composition of carbon and carbon-containing phases, it was important that there was only one carbon source in the experiments, namely, carbonate.

Optical and scanning electron microscopy and energy-dispersive spectroscopy

After termination of the experiments, the end products along with the diamond morphology were examined using both optical microscopy (Axio Imager Z2m optical microscope) and scanning electron microscopy (Tescan MIRA3 LMU SEM). For the energy-dispersive spectroscopy analysis, sections were prepared in the form of polished samples. Silicates and oxides were analyzed using a 20-kV accelerating voltage, a 20-nA probe current, 20-s counting time, and a 2- to 4-μm beam diameter. For carbonates and quenched carbonate-bearing melts, the accelerating voltage was lowered to 15 kV, probe current was lowered to 10 nA, the counting time was lowered to 10 s, and a defocused beam (diameter of 20 to 100 μm) was used. The analytical work described above was performed at the Center for Collective Use of Multi-Element and Isotopic Analysis of the SB RAS (Novosibirsk, Russia).

Raman spectroscopy

Raman spectra were recorded using a Horiba J.Y. LabRAM HR800 spectrometer coupled with an Olympus BX41 microscope. A diode-pumped solid-state laser emitting at 532 nm (Torus, Laser Quantum) was used as the excitation source. An Olympus 100 (numerical aperture, 0.90) objective was used to focus the laser beam onto the sample and to collect the Raman signal. The spectra were measured with a spectral resolution of 2 cm^{-1}. The spectrometer was calibrated using the emission lines at 540.06 and 585.25 nm of a neon gas discharge lamp. The accuracy of the band positioning in the Raman spectra was approximately 1 cm^{-1}.

IR spectroscopy

IR absorption spectra of diamonds were measured using a Bruker Vertex 70 FTIR (Fourier transform IR) spectrometer fitted with a Hyperion 2000 IR microscope. The spectra were acquired with a resolution of 2 cm^{-1} and averaging over 64 scans. Depending on the sample sizes, square apertures from 50 to 100 μm in width were used to collect spectra. The samples were placed onto a copper square mesh grids with proper hole sizes (125 μm by 125 μm or 90 μm by 90 μm). From the experiments where diamonds with sizes appropriate for micro-FTIR spectroscopy (≥100 μm) were produced, not less than 10 crystals were recovered and examined. The recorded spectra were converted to the absorption coefficient units by fitting to the standard IR spectrum of type IIa diamond so that to obtain the best fit of the intrinsic two-phonon absorption bands (2700 to 1700 cm^{-1}). Nitrogen concentrations were determined by deconvoluting the IR spectra, in the one-phonon region (1400 to 900 cm^{-1}), into A and C components and using conversion factors of 16.5 atomic ppm cm^{-1} of absorption at 1280 cm^{-1} for the A centers and 25 atomic ppm cm^{-1} of absorption at 1130 cm^{-1} for the C centers. The spectra were processed using a Bruker OPUS 6.5 software package. Because of the small sizes and irregular shapes of the crystallized diamonds, the recorded spectra were somewhat distorted by interference fringes and by relatively poor signal-to-noise ratios. This gave rise to some uncertainty in the fitting confidence, which was the major source of uncertainty in determining the absorption coefficients and, consequently, nitrogen concentrations. This uncertainty was sample dependent and is estimated to have varied by up to 20 to 25%.

Mass spectrometry

Carbon isotope composition of carbonates and graphite was measured using gas source isotope ratio mass spectrometry (IRMS) using a DELTA V Advantage instrument at the V.S. Sobolev Institute of Geology and Mineralogy (Novosibirsk). Graphite was oxidized in a vacuum-fused quartz reactor in the presence of pure CuO so as to produce CO_2 for IRMS analysis (*59*). Carbon from carbonates was thermally extracted at 950°C in a vacuum reactor before measurements. Isotopic reference materials NBS-18 (limestone), NBS-19 (calcite), and USGS-24 (graphite) with appropriate preparation were used for instrument calibration and to monitor data quality. The repeatability of $\delta^{13}C$ values on reference materials is better than 0.20‰ (2s).

The experimentally produced microdiamonds and graphite were investigated in situ for their $\delta^{13}C$ values using the CAMECA IMS 1280-HR secondary ion mass spectrometer (SIMS) at the GeoForschungsZentrum (GFZ) in Potsdam, Germany. Before the analyses, all samples were cast in indium metal together with relevant reference materials of known compositions using a hand-operated press. The surface of the 2.54 cm sample mounts was then cleaned using high-purity ethanol before being argon sputter-coated with a 35-nm-thick, high-purity gold film.

SIMS analyses used $^{133}Cs^+$ primary beam with a total impact energy of 20 keV. The Gaussian primary ion beam with a 2.0-nA current was focused to a 4- to 8-μm-diameter spot on the sample surface. Secondary ions were extracted using a −10-kV potential applied to the sample holder. Charge compensation involved circa 250-pA, low-energy electron cloud provided by a normal-incidence electron

flood gun. The instrument was operated with a circa 80-μm field of view and a 40-eV wide energy window. We used static multicollection mode operating at a mass resolution of $M/\Delta M \approx 3200$ at the 13-Da mass station, which fully resolved ^{13}C from the nearby $^{12}C^{1}H$ molecular isobar. Machine calibration used two synthetic diamond reference materials contained in the same indium-based sample mount: crystal 140/4 with $\delta^{13}C_{VPDB} = 26.5‰$ and crystal 150/3 with $\delta^{13}C_{VPDB} = 24.5‰$ (*60*, *61*). For isotope measurements on graphite, a natural graphite called RM18 with $\delta^{13}C = -7.01‰$ Vienna Pee Dee belemnite (VPDB) (determined in V.S. Sobolev Institute of Geology and Mineralogy, SB RAS using gas source IRMS following method described above) was used as our reference material. Overall isotope homogeneity of RM18, based on more than 50 random location measurements, is better than ±0.5‰. No significant time-dependent linear drift was observed during our SIMS measurements. The repeatability of the $^{13}C/^{12}C$ determinations on restricted area of the reference material was better than 0.24‰ (2s), which is our best estimate for the random component that might be present in our data.

SUPPLEMENTARY MATERIALS

Supplementary material for this article is available at http://advances.sciencemag.org/cgi/content/full/7/4/eabb4644/DC1

REFERENCES AND NOTES

1. S. E. Haggerty, A diamond trilogy: Superplumes, supercontinents, and supernovae. *Science* **285**, 851–860 (1999).
2. T. Stachel, G. P. Brey, J. W. Harris, Inclusions in sublithospheric diamonds: Glimpses of deep Earth. *Elements* **1**, 73–78 (2005).
3. T. Stachel, T. Chacko, R. W. Luth, Carbon isotope fractionation during diamond growth in depleted peridotite: Counterintuitive insights from modelling water-maximum CHO fluids as multi-component systems. *Earth Planet. Sci. Lett.* **473**, 44–51 (2017).
4. S. B. Shirey, P. Cartigny, D. J. Frost, S. Keshav, F. Nestola, P. Nimis, G. D. Pearson, N. V. Sobolev, M. J. Walter, Diamonds and the geology of mantle carbon. *Rev. Mineral. Geochem.* **75**, 355–421 (2013).
5. S. B. Shirey, K. V. Smit, G. D. Pearson, M. J. Walter, S. Aulbach, F. E. Brenker, H. Bureau, A. D. Burnham, P. Cartigny, T. Chacko, D. J. Frost, E. H. Hauri, D. E. Jacob, S. D. Jacobsen, S. C. Kohn, R. W. Luth, S. Mikhail, O. Navon, F. Nestola, P. Nimis, M. Palot, E. M. Smith, T. Stachel, V. Stagno, A. Steele, R. A. Stern, E. Thomassot, A. R. Thomson, Y. Weiss. Diamonds and the mantle geodynamics of carbon, in *Deep Carbon* (Cambridge, 2019), chap. 5, pp. 89–128.
6. T. Stachel, J. W. Harris, The origin of cratonic diamonds—Constraints from mineral inclusions. *Ore Geol. Rev.* **34**, 5–32 (2008).
7. O. Navon, I. D. Hutcheon, G. R. Rossman, G. J. Wasserburg, Mantle-derived fluids in diamond micro-inclusions. *Nature* **335**, 784–789 (1988).
8. O. Klein-BenDavid, A. M. Logvinova, M. Schrauder, Z. V. Spetius, Y. Weiss, E. H. Hauri, F. V. Kaminsky, N. V. Sobolev, O. Navon, High-Mg carbonatitic microinclusions in some Yakutian diamonds—A new type of diamond-forming fluid. *Lithos* **112**, 648–659 (2009).
9. L. F. Dobrzhinetskaya, R. Wirth, H. W. Green II, A look inside of diamond-forming media in deep subduction zones. *Proc. Natl. Acad. Sci. U.S.A.* **104**, 9128–9132 (2007).
10. E. L. Tomlinson, A. P. Jones, J. W. Harris, Co-existing fluid and silicate inclusions in mantle diamond. *Earth Planet. Sci. Lett.* **250**, 581–595 (2006).
11. Y. N. Pal'yanov, A. G. Sokol, Y. M. Borzdov, A. F. Khokhryakov, N. V. Sobolev, Diamond formation from mantle carbonate fluids. *Nature* **400**, 417–418 (1999).
12. E. M. Smith, S. B. Shirey, F. Nestola, E. S. Bullock, J. Wang, S. H. Richardson, W. Wang, Large gem diamonds from metallic liquid in Earth's deep mantle. *Science* **354**, 1403–1405 (2016).
13. K. V. Smit, S. B. Shirey, R. A. Stern, A. Steele, W. Wang, Diamond growth from C–H–N–O recycled fluids in the lithosphere: Evidence from CH_4 micro-inclusions and $\delta^{13}C$–$\delta^{15}N$–N content in Marange mixed-habit diamonds. *Lithos* **265**, 68–81 (2016).
14. K. A. Smart, P. Cartigny, S. Tappe, H. O'Brien, S. Klemme, Lithospheric diamond formation as a consequence of methane-rich volatile flooding: An example from diamondiferous eclogite xenoliths of the Karelian craton (Finland). *Geochim. Cosmochim. Acta* **206**, 312–342 (2017).
15. F. Piccoli, J. Hermann, T. Pettke, J. A. D. Connolly, E. D. Kempf, J. F. Vieira Duarte, Subducting serpentinites release reduced, not oxidized, aqueous fluids. *Sci. Rep.* **9**, 19573 (2019).
16. H. Bureau, D. J. Frost, N. Bolfan-Casanova, C. Leroy, I. Esteve, P. Cordier, Diamond growth in mantle fluids. *Lithos* **265**, 4–15 (2016).
17. D. A. Sverjensky, F. Huang, Diamond formation due to a pH drop during fluid–rock interactions. *Nat. Commun.* **6**, 8702 (2015).
18. F. Kaminsky, Mineralogy of the lower mantle: A review of 'super-deep' mineral inclusions in diamond. *Earth Sci. Rev.* **110**, 127–147 (2012).
19. Y. N. Palyanov, Y. V. Bataleva, A. G. Sokol, Y. M. Borzdov, I. N. Kupriyanov, N. V. Reutsky, N. V. Sobolev, Mantle–slab interaction and redox mechanism of diamond formation. *Proc. Natl. Acad. Sci. U.S.A.* **110**, 20408–20413 (2013).
20. S. M. Dorfman, J. Badro, F. Nabiei, V. B. Prakapenka, M. Cantoni, P. Gillet, Carbonate stability in the reduced lower mantle. *Earth Planet. Sci. Lett.* **489**, 84–91 (2018).
21. A. R. Thomson, M. J. Walter, S. C. Kohn, R. A. Brooker, Slab melting as a barrier to deep carbon subduction. *Nature* **529**, 76–79 (2016).
22. T. Stachel, R. W. Luth, Diamond formation—Where, when and how? *Lithos* **220–223**, 200–220 (2015).
23. R. Luth, Diamond formation during partial melting in the Earth's mantle. *Abstr. Progr. – Geol. Soc. Amer.* **49**, 20–26 (2017).
24. K. V. Smit, T. Stachel, R. W. Luth, R. A. Stern, Evaluating mechanisms for eclogitic diamond growth: An example from Zimmi Neoproterozoic diamonds (West African craton). *Chem. Geol.* **520**, 21–32 (2019).
25. M. Arima, Y. Kozai, M. Akaishi, Diamond nucleation and growth by reduction of carbonate melts under high-pressure and high-temperature conditions. *Geology* **30**, 691–694 (2002).
26. J. Siebert, F. Guyot, V. Malavergne, Diamond formation in metal–carbonate interactions. *Earth Planet. Sci. Lett.* **229**, 205–216 (2005).
27. S. Yamaoka, M. D. S. Kumar, H. Kanda, M. Akaishi, Formation of diamond from $CaCO_3$ in a reduced C–O–H fluid at HP–HT. *Diamond Relat. Mater.* **11**, 1496–1504 (2002).
28. Y. N. Pal'yanov, A. G. Sokol, Y. M. Borzdov, A. F. Khokhryakov, N. V. Sobolev, Diamond formation through carbonate-silicate interaction. *Amer. Mineral.* **87**, 1009–1013 (2002).
29. Y. N. Palyanov, Y. M. Borzdov, Y. V. Bataleva, A. G. Sokol, G. A. Palyanova, I. N. Kupriyanov, Reducing role of sulfides and diamond formation in the Earth's mantle. *Earth Planet. Sci. Lett.* **260**, 242–256 (2007).
30. S. C. Gunn, R. W. Luth, Carbonate reduction by Fe–S–O melts at high pressure and high temperature. *Am. Mineral.* **91**, 1110–1116 (2006).
31. T. Yoshino, B. Gruber, C. Reinier, Effects of pressure and water on electrical conductivity of carbonate melt with implications for conductivity anomaly in continental mantle lithosphere. *Phys. Earth Planet. Inter.* **281**, 8–16 (2018).
32. S. Ono, K. Mibe, Influence of pressure and temperature on the electrical conductivity of dolomite. *Phys Chem Minerals* **42**, 773–779 (2015).
33. A. Pommier, E. J. Garnero, Petrology-based modeling of mantle melt electrical conductivity and joint interpretation of electromagnetic and seismic results. *J. Geophys. Res. Solid Earth* **119**, 4001–4016 (2014).
34. A. E. Ringwood, On the chemical evolution and densities of the planets. *Geochim. Cosmochim. Acta* **15**, 257–283 (1959).
35. F. Gaillard, M. Malki, G. Iacono-Marziano, M. Pichavant, B. Scaillet, Carbonatite melts and electrical conductivity in the asthenosphere. *Science* **322**, 1363–1365 (2008).
36. A. Kavner, D. Walker, Core/mantle-like interactions in an electric field. *Earth Planet. Sci. Lett.* **248**, 316–329 (2006).
37. D. C. Tozer, in *Physics and Chemistry of the Earth*, K. Rankama, S. K. Runcorn, Eds. (Pergamon Press, 1959) vol. 3, pp. 414–436.
38. T. Rikitate, *Electromagnetism and the Earth's Interior* (Elsevier, Amsterdam, 1966).
39. D. J. Frost, C. A. McCammon, The redox state of Earth's mantle. *Annu. Rev. Earth Planet. Sci.* **36**, 389–420 (2008).
40. V. Stagno, Y. Fei, The redox boundaries of Earth's interior. *Elements* **16**, 167–172 (2020).
41. T. Chacko, D. R. Cole, J. Horita, Equilibrium oxygen, hydrogen and carbon isotope fractionation factors applicable to geologic systems. *Rev. Miner. Geochem.* **43**, 1–81 (2001).
42. Y. Moussallam, P. Florian, D. Corradini, Y. Morizet, N. Sator, R. Vuilleumier, B. Guillot, G. Lacono-Marziano, B. C. Schmidt, F. Gaillard, The molecular structure of melts along the carbonatite–kimberlite–basalt compositional joint: CO_2 and polymerisation. *Earth Planet. Sci. Lett.* **434**, 129–140 (2016).
43. B. Mysen, Redox-controlled mechanisms of C and H isotope fractionation between silicate melt and COH fluid in the Earth's interior. *Progr. Earth Planet. Sci.* **5**, 46 (2018).
44. M. D. Ingram, B. Baron, G. J. Janz, The electrolytic deposition of carbon from fused carbonates. *Electroch. Acta* **11**, 1629–1639 (1966).
45. H. V. Ijije, R. C. Lawrence, G. Z. Chen, Carbon electrode position in molten salts: Electrode reactions and applications. *RSC Adv.* **4**, 35808–35817 (2014).
46. P. J. Wyllie, W. L. Huang, High CO_2 solubilities in mantle magmas. *Geology* **4**, 21–24 (1976).
47. G. P. Brey, I. D. Ryabchikov, Carbon dioxide in strongly silica undersaturated melts and origin of kimberlite magmas. *Neus. Jb. Miner. Mh.* **10**, 449–463 (1994).

48. Y. N. Palyanov, I. N. Kupriyanov, A. G. Sokol, Y. M. Borzdov, A. F. Khokhryakov, Effect of CO_2 on crystallization and properties of diamond from ultra-alkaline carbonate melt. *Lithos* **265**, 339–350 (2016).
49. Y. N. Pal'yanov, A. G. Sokol, A. A. Tomilenko, N. V. Sobolev, Conditions of diamond formation through carbonate-silicate interaction. *Eur. J. Mineral.* **17**, 207–214 (2005).
50. T. Plank, C. E. Manning, Subducting carbon. *Nature* **574**, 343–352 (2019).
51. R. Dasgupta, M. M. Hirschmann, The deep carbon cycle and melting in Earth's interior. *Earth Planet. Sci. Lett.* **298**, 1–13 (2010).
52. A. Kavner, A. Shahar, F. Bonet, J. Simon, E. Young, The isotopic effects of electron transfer: An explanation for Fe isotope fractionation in nature. *Geochim. Cosmochim. Acta* **69**, 2971–2979 (2005).
53. V. Reutsky, Y. Borzdov, Y. Palyanov, A. Sokol, O. Izokh, Carbon isotope fractionation during experimental crystallisation of diamond from carbonate fluid at mantle conditions. *Contrib. Mineral. Petrol.* **170**, 41 (2015).
54. A. Kavner, D. Walker, S. Sutton, M. Newville, Externally-driven charge transfer in silicates at high pressure and temperature: A XANES study. *Earth Planet. Sci. Lett.* **256**, 314–327 (2007).
55. B. Debret, D. A. Sverjensky, Highly oxidising fluids generated during serpentinite breakdown in subduction zones. *Sci. Rep.* **7**, 10351 (2017).
56. Y. Palyanov, I. Kupriyanov, A. Khokhryakov, V. Ralchenko, Crystal Growth of Diamond, in *Handbook of Crystal Growth*, T. Nishinaga, P. Rudolph, Eds. (Elsevier, 2015), vol. II, chap.17, pp. 671–713.
57. Y. N. Pal'yanov, A. G. Sokol, M. Borzdov, A. F. Khokhryakov, Fluid-bearing alkaline carbonate melts as the medium for the formation of diamonds in the Earth's mantle: An experimental study. *Lithos* **60**, 145–159 (2002).
58. A. G. Sokol, Y. M. Borzdov, Y. N. Palyanov, A. F. Khokhryakov, High-temperature calibration of a multianvil high pressure apparatus. *High Press. Res.* **35**, 139–147 (2015).
59. V. N. Reutsky, Y. M. Borzdov, Y. N. Palyanov, Effect of diamond growth rate on carbon isotope fractionation in Fe–Ni–C system. *Diamond Relat. Mater.* **21**, 7–10 (2012).
60. V. N. Reutsky, B. Harte, Y. M. Borzdov, Y. N. Palyanov, Monitoring diamond crystal growth, a combined experimental and SIMS study. *Eur. J. Mineral.* **20**, 365–374 (2008).
61. V. N. Reutsky, P. M. Kowalski, Y. N. Palyanov, M. Wiedenbeck, Experimental and theoretical evidence for surface-induced carbon and nitrogen fractionation during diamond crystallization at high temperatures and high pressures. *Crystals* **7**, 190 (2017).

Acknowledgments: We thank N. S. Karmanov and M. V. Khlestov for consultations and assistance with scanning electron microscopy and energy dispersive analysis, as well as D. V. Nechaev and I. D. Novoselov for sample preparation and taking optical micrographs. F. Couffignal is thanked for support in running the SIMS analyses. **Funding:** This work was supported by the Russian Science Foundation under grant no. 19-17-00075. **Author contributions:** Y.N.P., Y.M.B., A.G.S., and N.V.S. designed the research. Y.N.P., Y.M.B., Y.V.B., and I.N.K. carried out the research. Y.M.B. and A.G.S. performed the HPHT experiments. Y.V.B. performed the scanning electron microscopy and energy-dispersive spectrometry analyses. Y.N.P., Y.V.B., I.N.K., and V.N.R. analyzed data. I.N.K. performed the IR and Raman spectroscopy. V.N.R. and M.W. performed the mass spectrometry. Y.V.B. and I.N.K. performed image processing. Y.N.P., Y.V.B., I.N.K., V.N.R., M.W., and N.V.S. wrote the paper. **Competing interests:** The authors declare that they have no competing interests. **Data and materials availability:** All data needed to evaluate the conclusions in the paper are present in the paper and/or the Supplementary Materials. Additional data related to this paper may be requested from the authors.

Submitted 26 February 2020
Accepted 1 December 2020
Published 20 January 2021
10.1126/sciadv.abb4644

Citation: Y. N. Palyanov, Y. M. Borzdov, A. G. Sokol, Y. V. Bataleva, I. N. Kupriyanov, V. N. Reutsky, M. Wiedenbeck, N. V. Sobolev, Diamond formation in an electric field under deep Earth conditions. *Sci. Adv.* **7**, eabb4644 (2021).

Diamond formation in an electric field under deep Earth conditions

Yuri N. Palyanov, Yuri M. Borzdov, Alexander G. Sokol, Yuliya V. Bataleva, Igor N. Kupriyanov, Vadim N. Reutsky, Michael Wiedenbeck and Nikolay V. Sobolev

Sci Adv **7** (4), eabb4644.
DOI: 10.1126/sciadv.abb4644